Giant Rabi splitting at the phonon line within all-semiconductor metallic-insulator-metallic antennas

Rafik Smaali, Fatima Omeis, Emmanuel Centeno, Thierry Taliercio, F Gonzalez-Posada, L Cerutti

▶ **To cite this version:**

Rafik Smaali, Fatima Omeis, Emmanuel Centeno, Thierry Taliercio, F Gonzalez-Posada, et al.. Giant Rabi splitting at the phonon line within all-semiconductor metallic-insulator-metallic antennas. Physical Review B, 2019, 100 (4), pp.041302. 10.1103/physrevb.100.041302 . hal-04047695

HAL Id: hal-04047695
https://hal.science/hal-04047695

Submitted on 27 Mar 2023

HAL is a multi-disciplinary open access archive for the deposit and dissemination of scientific research documents, whether they are published or not. The documents may come from teaching and research institutions in France or abroad, or from public or private research centers.

L'archive ouverte pluridisciplinaire **HAL**, est destinée au dépôt et à la diffusion de documents scientifiques de niveau recherche, publiés ou non, émanant des établissements d'enseignement et de recherche français ou étrangers, des laboratoires publics ou privés.

Rapid Communications

Giant Rabi splitting at the phonon line within all-semiconductor metallic-insulator-metallic antennas

Rafik Smaali, Fatima Omeis, and Emmanuel Centeno*
Université Clermont Auvergne, CNRS, SIGMA Clermont, Institut Pascal, F-63000 Clermont-Ferrand, France

Thierry Taliercio, F. Gonzalez-Posada, and L. Cerutti
Université Montpellier, CNRS, IES, UMR 5214, F-34000 Montpellier, France

(Received 8 March 2019; revised manuscript received 26 June 2019; published 8 July 2019)

We experimentally demonstrate an ultrastrong coupling regime between a gap plasmon and phonon in metallic-insulator-metallic antennas at far-infrared frequencies. These plasmonic antennas made of a silicon-doped semiconductor (InAsSb) are versatile structures able to reveal the polaritonic modes due to the hybridization of a gap plasmon and phonon. The anticrossing behavior featuring the ultrastrong coupling is properly studied by varying the width of the metallic antenna array. The gap-plasmon resonance supported by the antennas is shown to be particularly sensitive to the presence of phonons in the GaSb insulator. The experimental data demonstrate a giant Rabi splitting of 30% of the GaSb transverse optical phonon energy and are in good agreement with both electromagnetic and semiclassical calculations.

DOI: 10.1103/PhysRevB.100.041302

Confining electromagnetic waves (EW) beyond the diffraction limit with plasmonic systems attracts a lot of attention owing to the possibility of conceiving dense and efficient photonic components [1]. We are currently witnessing a growing demand for plasmonic components operating in the far-infrared (Far-IR) and the terahertz (THz) range to address the challenges posed by several domains such as security, imaging, sensing, and biomedical [2–6]. In view of proposing integrated photonic devices, efforts have focused on metal alloys [7], heavily doped semiconductors [8,9], and more recently, graphene [10] in order to replace noble metals which are not compatible with silicon technology [not complementary metal-oxide semiconductor (CMOS) compatible]. Heavily doped semiconductors (HDSC) are promising since, in addition to their CMOS compatibility, their optical properties can be adjusted on demand by controlling the doping level [11–14]. Among the different geometries explored to reveal plasmonic effects, metal-insulator-metal (MIM) structures have been proved to boost the Purcell factor and the light extraction or to behave as perfect and tunable absorbers [15–19]. MIM antennas support a specific plasmonic mode named gap plasmon, which is a propagating electromagnetic wave squeezed into a subwavelength gap between two metals [20–24]. MIM antennas constitute also an ideal structure to test extreme interactions between photons and electrons. When the gap is reduced to only some hundredths of a wavelength, very high wave vectors are reached for the gap-plasmon mode allowing one to reveal the nonlocal behavior for electrons [25–27]. MIM antennas made of HDSC and operating in the Far-IR have been experimentally studied and show similar efficiencies to their noble metal counterpart [28,29].

In this Rapid Communication, we experimentally demonstrate that the resonant frequency of MIM antennas can be shifted to the phonon frequency of the insulator giving rise to strong coupling between the phonon and gap plasmon. This quasiparticle that we name gap-plasmon-phonon-polariton (G3P), is the result of an ultrastrong interaction of light with the matter within a subwavelength cavity. Classical and quantum theories show that MIM antennas made of HDSC constitute a versatile platform for realizing a giant Rabi splitting up to 30% of the phonon energy.

Usually, polaritons are obtained with an active material inserted into an optical resonator. Extensively studied, microcavity polaritons have led to a new field in photonics [30–32]. The strength of the interaction is evaluated by the ratio η between the vacuum field Rabi splitting E_R and the bare energy of the excitations E_c. Weak and strong coupling regimes correspond to $\eta < 10\%$. For the ultrastrong coupling (USC) regime η spans from 10% to 100%, and the deep strong coupling regime is attained beyond $\eta = 100\%$ [33]. The USC has been already observed in several systems and at different wavelengths. The first observation of the USC was with the intersubband polaritons [34], then in the superconducting circuits [35], the Landau polaritons [36], the organic molecules [37], and much more recently the optomechanical systems [38]. Contrarily to the weak and strong coupling regimes, the USC is less sensitive to the dissipation and decoherence effects that affect the quantum properties of the quantum states [33]. In addition, the USC regime boosts nonlinear effects and strongly affects the kinetics of a chemical reaction [39]. Several studies have demonstrated the possibility to couple phonons and photons in plasmonic structures. Part of them deals with localized surface plasmons exploiting

*emmanuel.centeno@uca.fr

 ©2019 American Physical Society

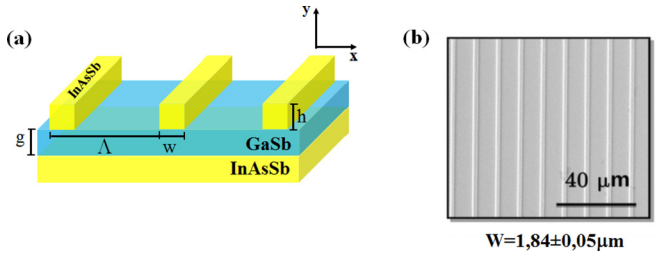

FIG. 1. (a) Schematic of the MIM structure. (b) SEM image of the top view of MIM antennas.

the gap-plasmon or lightning rod effect that couple with the phonon mode of inorganic material, SiO_2, [40,41], or with an organic material such as the polymethyl methacrylate vibrational mode [42] or molecular vibrations of a benzonitrile solution [43]. In the latter, an optical microcavity was used. All these experimental demonstrations were realized in the strong coupling regime except the case of the thickest SiO_2 layer in [41], but this work was not discussed in terms of USC. MIM antennas based on gold has been used to observe USC with intersubband polaritons but not directly with phonons because alloys present a too complex phonon band structure [44,45].

Our work demonstrates that a MIM antenna made of HDSC is an ideal system for revealing the USC between the phonon and the gap-plasmon modes. The gap-plasmon mode resulting yet from a strong interaction of photons and electrons is particularly sensitive to other resonances that occur within the insulation spacer embedded into the MIM antenna. Here the MIM resonators consist of a GaSb dielectric spacer of thickness $g = 0.6\ \mu$m sandwiched between a back mirror and a periodic set of ribbons made of silicon-doped $InAs_{0.9}Sb_{0.1}$. Large periods for the arrays of $\wedge = 9$ and 12 μm, that correspond to about three to five times the ribbon width w are used to minimize the electromagnetic coupling between adjacent MIM antennas [Fig. 1(a)]. The MIM layered structures have been grown by solid source molecular beam epitaxy (RIBER, compac 21 growth chamber). After an oxide desorption of the Te-doped (100)-GaSb substrate, three layers of 993 nm of Si-doped $InAs_{0.9}Sb_{0.1}$, 630 nm of nonintentionally doped GaSb, and 298 nm of Si-doped $InAs_{0.9}Sb_{0.1}$ have been grown lattice matched to the substrate. The carrier concentration of the Si-doped $InAs_{0.9}Sb_{0.1}$ is 5×10^{19} cm^{-3} guaranteeing a metallic behavior for frequency lower than 54 THz (or 1800 cm^{-1}). The antennas are fabricated by laser lithography and wet chemical etching in the top layer of heavily doped n-$InAs_{0.9}Sb_{0.1}$. The laser lithography consists of a direct writing with an ultraviolet laser at $\lambda = 365$ nm of a AZMIR-701 photoresist spun at 4000 rpm for 30 s and heated at 90 °C for 1 min. The fabricated samples are 2×2 mm^2 surfaces with different periods and antenna widths. A scanning electron microscopy (SEM) image of the structure is shown in Fig. 1(b).

The reflectance spectra are performed using a Bruker V70 Fourier transform infrared spectrometer equipped with a potassium bromide beam splitter, a Hg far-infrared source, and a Si-bolometer detector cooled at 4.2 K. The experimental setup covers the spectral range from 15 to 55 μm. The

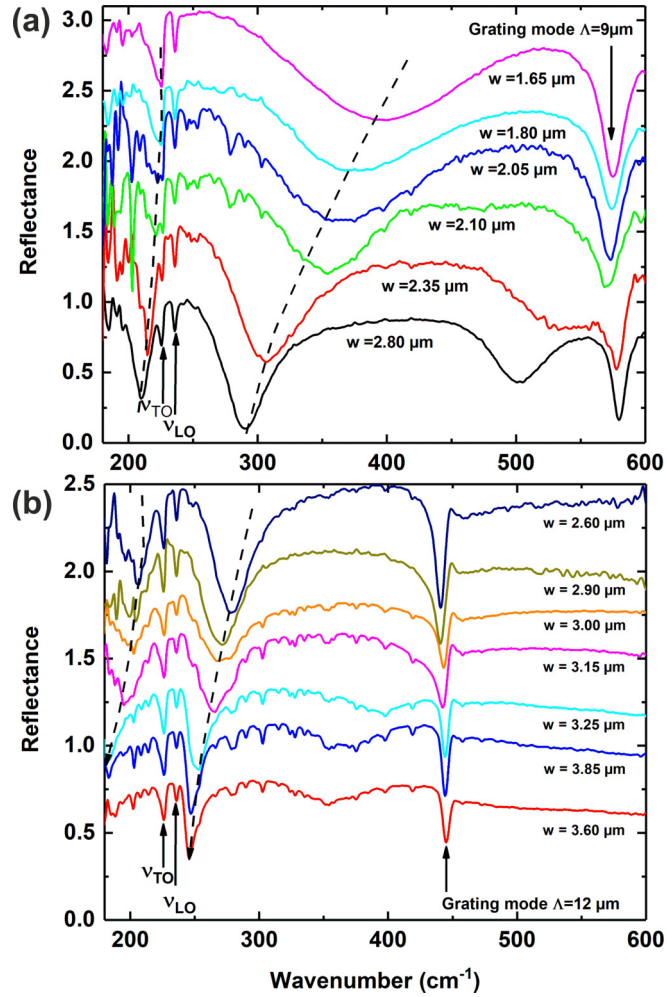

FIG. 2. Experimental reflection spectra plotted for samples A and B with different ribbon widths (accuracy is 0.05 μm). The antenna array periodicities of samples A and B are, respectively, (a) 9 μm and (b) 12 μm. Curves are vertically translated for clarity. The dashed lines are a guide for the eyes and indicate the evolution of the gap-plasmon hybridization. Vertical arrows show the wave numbers of the TO- and LO-phonon lines and the first-order mode of the grating.

incident EW makes a 60° angle against the normal and is polarized by a holographic wire grid. A mask is used to limit the sample surface and avoid any reflected light from unprocessed parts of the samples. The oblique incidence configuration provides access to all photonic modes and notably to the transverse optic (TO) and longitudinal optic (LO) phonon resonances thanks to the Berreman effect [46].

Figure 2 represents the measured reflectance spectra for samples A and B with, respectively, two antenna arrays of periodicity 9 and 12 μm. Each spectrum corresponds to a ribbon width w. We observe that the full width at half maximum (FWHM) of the G3P absorption lines are deeply affected by the ribbon width. Grating modes, indicated by the vertical arrows, appear at different wave numbers 580 and 445 cm^{-1} according to the periods. As previously mentioned, the gap-plasmon resonance is governed by the width of the antenna. For example, very similar spectra are obtained for

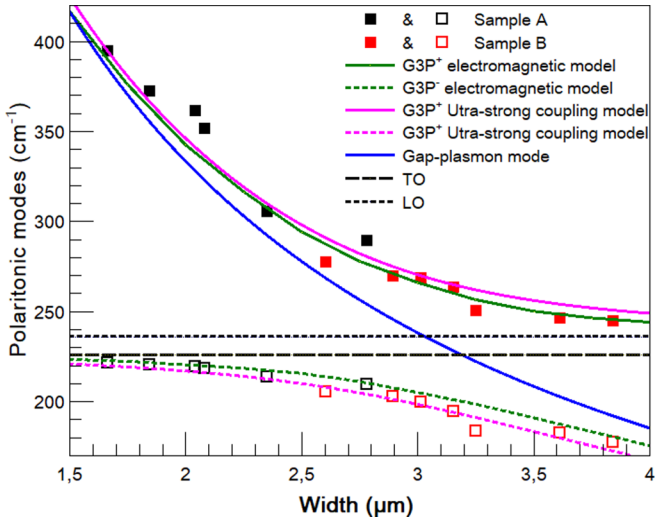

FIG. 3. Resonant frequencies in wave-number units versus the antenna width for the G3P modes extracted from the experiments data. The dotted and dashed lines are, respectively, for LO- and TO-phonon resonances. The blue curve corresponds to the uncoupled gap-plasmon mode. The green and magenta curves are the $G3P^+$ (solid line) and $G3P^-$ (dotted line) resonances calculated respectively with the electromagnetic simulations and the ultrastrong coupling model.

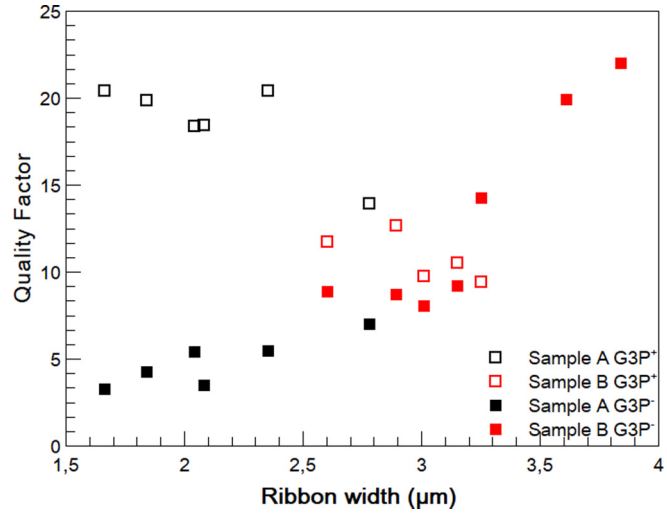

FIG. 4. Quality factor extracted from experimental data $Q_{ex} = \nu_{G3P}/\mathrm{FWHM}$ as a function of the width w for both G3P resonances.

both lattice periods 9 and 12 μm for similar widths, $w = 2.80$ μm in Fig. 2(a), and $w = 2.60$ μm in Fig. 2(b). The phonon resonances at the wave numbers ν_{LO} and ν_{TO} are visible on the spectra since the gap plasmon is confined within the antenna which allows the incident EW to couple directly with the exposed GaSb surface (about 65%–75% of the total area).

To demonstrate the strong coupling regime between the gap plasmon and the phonons, the G3P resonances extracted from the experimental spectra are represented in wave-number units as a function of the ribbon width (open and solid red squares, Fig. 3). An anticrossing behavior is recognized around the phonon reststrahlen band, which is represented by the dark dotted and dashed lines. The hybridization of the gap plasmon with the phonons is confirmed by the reflection spectra calculated for a TM polarized plane wave presenting an incident angle of 60° (corresponding to the experimental measurement) with a homemade code based on the rigorous coupled wave analysis method [47]. The optical properties of the materials are implemented with a Lorentz model for GaSb and a Drude-Lorentz model for InAsSb. The relative permittivities ϵ_d and ϵ_m respectively for GaSb and InAsSb read

$$\epsilon_d = \epsilon_\infty\left(1 + \frac{\omega_{LO}^2 - \omega_{TO}^2}{\omega_{TO}^2 - \omega^2 - i\omega\Gamma}\right), \quad (1)$$

$$\epsilon_m = \tilde{\epsilon}_\infty\left(1 - \frac{\omega_p^2}{\omega(\omega + i\gamma)}\right) + \tilde{\epsilon}_\infty\left(\frac{\tilde{\omega}_{LO}^2 - \tilde{\omega}_{TO}^2}{\tilde{\omega}_{TO}^2 - \omega^2 - i\omega\tilde{\Gamma}}\right), \quad (2)$$

where the GaSb material parameters are $\epsilon_{\mathrm{GaSb}} = 14.4$, $\omega_{LO} = 43.9 \times 10^{12}$ rad s^{-1}, $\omega_{TO} = 42.2 \times 10^{12}$ rad s^{-1}, $\Gamma = 0.56 \times 10^{12}$ rad s^{-1} and those of InAsSb are $\tilde{\omega}_{LO} = 44 \times 10^{12}$ rad s^{-1}, $\tilde{\omega}_{TO} = 40.4 \times 10^{12}$ rad s^{-1}, $\tilde{\Gamma} = 0.56 \times 10^{12}$ rad s^{-1}. The parameters for the Drude model experimentally determined by measuring the Brewster mode are $\tilde{\epsilon}_\infty = 11.4$, $\gamma = 10^{13}$ rad s^{-1}, and the plasma frequency $\omega_p = 3.51 \times 10^{14}$ rad s^{-1} [48]. Phonons into the InAsSb are screened due to the high free carrier density, whereas those into the GaSb drastically modified the scenario when they coupled with the gap plasmon. Since the gap plasmon propagates within the spacer, it is extremely sensitive to the phonon resonances of GaSb. This behavior is confirmed by the calculations of the resonant frequencies of the MIM antennas with and without the phonon term of Eq. (1). Without the phonons in the GaSb layer, the gap-plasmon resonance shifts over the entire frequency band (blue curve) when the width of the antenna is varied (Fig. 3). This behavior agrees with a cavity model for the MIM antenna that expresses the resonant wavelength as

$$\lambda_r = 2n_{\mathrm{eff}}w + \lambda_\phi, \quad (3)$$

where the effective index of the gap plasmon is $n_{\mathrm{eff}} = k_x/k_0$ (k_x being is the propagation constant and k_0 the wave number in vacuum) and λ_ϕ is a correction that takes into account the coupling with the incident field [28,49,50]. This picture is drastically modified when the EW simulations integrate the phonon resonances described by Eq. (1) for the GaSb layer. In that case, the gap plasmon strongly interacts with the phonons leading to the anticrossing experimentally observed (green curves, Fig. 3). The Rabi splitting, the minimum energy between both G3P modes, reaches 30% of the TO-phonon wave number for an antenna width of 3.1 μm. The complete picture of the gap-plasmon and phonon coupling is depicted in Fig. 5(a) by the simulated reflectance as a function of the antenna width and the wave number. The strong coupling regime is also assessed by the modification of the quality factor of the MIM antenna due to its hybridization with the phonon mode. The experimental quality factor $Q_{ex} = \nu_{G3P}/\mathrm{FWHM}$ is plotted as a function of the width w for both G3P resonances in Fig. 4. The experimental data of the $G3P^-$ mode are out of range for antenna widths larger than 3.4 μm. At the maximum of strong coupling ($w = 3.1$ μm) both G3P resonances present

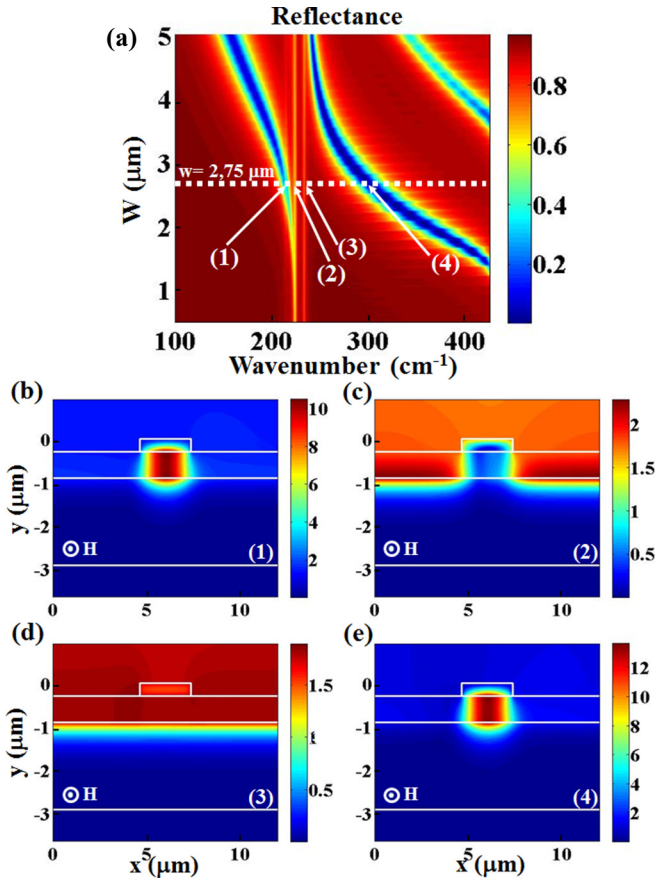

FIG. 5. (a) Reflectance spectra as a function of the wave number and the antenna's width. (b)–(e) Maps of the magnetic field modulus calculated for each absorption line labeled in panel (a).

equal Q_{ex} since in this regime the G3P quasiparticles are equally mixed, half gap plasmon and half phonon. Far from this anticrossing, for a small antenna width around $w = 1.6\ \mu$m, their quality factors differ by a factor of 4. Here, the $G3P^-$ is a phononlike resonance with a large Q_{ex} while the $G3P^+$ is a gap-plasmon-like resonance with a small Q_{ex}. The opposite situation is observed for a large antenna width. This behavior is reproduced for the theoretical quality factor Q_{th} obtained with the electromagnetic simulations (not shown in Fig. 4). Q_{th} is two times larger than Q_{ex} suggesting that additional losses attributed to the fabrication process degrade the electromagnetic confinement of the MIM antennas.

The hybridization of the gap plasmon is also clearly identified on the map of the modulus of the magnetic field calculated for a width $w = 2.75\ \mu$m [Figs. 5(b)–5(e)]. The magnetic field profiles calculated for the absorption lines labeled (1) and (4) correspond, respectively, to the $G3P^-$ and $G3P^+$ modes [Figs. 5(b) and 5(e)]. The G3P+ looks like a gap plasmon trapped underneath the ribbon when its resonance frequency is situated far from that of the phonons [Fig. 5(e)]. The $G3P^-$ is less localized than the $G3P^+$ as assessed by its weaker maximal value and spreads within the GaSb spacer showing that the gap plasmon better interacts with the phonons [Fig. 5(b)]. The transverse and longitudinal phonon resonances cause the weak absorption lines that correspond to Fabry-Perot resonances within the GaSb layer [see Figs. 5(c) and 5(d)]. Figure 5(d) corresponds to the Berreman mode with the enhancement of the magnetic field everywhere in the GaSb spacer.

Beyond the good agreement of the experimental data and electromagnetic simulations, we described the gap-plasmon and phonons coupling in the framework of a semiclassical theory. However, the choice of the most adapted model is not so easy. Indeed, the strong coupling regime features an anticrossing effect but not a frequency gap opening for any wave number between the upper and the lower polariton branches, i.e., in the reststrahlen band. A semiclassical strong coupling model gives a good agreement except for the $G3P^+$ and the $G3P^-$ modes that reach asymptotically the wrong TO- or the LO-phonon energies and not the actual LO- and TO-phonon branches. To feature this energy gap, it is necessary to consider an ultrastrong coupling model. The two uncoupled states are the LO-phonon $|P\rangle$ and the gap-plasmon $|GP\rangle$ levels with respective energy $E_P = \hbar\omega_{LO_{\mathrm{GaSb}}}$ and $E_{GP} = hc/\lambda_r$ where c is the speed of light in vacuum and λ_r is given by Eq. (3) (with $n_{\mathrm{eff}} = 6$ and $\lambda_\phi = 6\ \mu$m). The strength of the coupling between both states is the Rabi energy $E_R = \eta E_P$. The diagonalization of the light-matter Hamiltonian in the dipole gauge [51] gives the secular equation

$$\left(E^2 - E_P^2\right)\left(E^2 - E_{GP}^2\right) = E_R^2 E_{GP}^2. \tag{4}$$

The solutions of Eq. (4) are the $G3P$ dispersion curves drawn in Fig. 3 (magenta dashed and solid lines). These theoretical results are in good agreement with the experimental data confirming thus the ultrastrong coupling. The asymptotical values for large and small ribbon's width of the $G3P^+$ and $G3P^-$ modes are, respectively, the LO- and TO-phonon modes. The reststrahlen band appears between the upper and lower polariton branches. The unique adjustable parameter of the model is the Rabi energy which is 30% of the LO-phonon energy (corresponding to $\eta = 0.3$), in agreement with the giant value experimentally observed. The root-mean-square fit value of the ultrastrong model is improved by 12% compared to the electromagnetic model.

In conclusion, we have experimentally demonstrated a hybridization of gap plasmon with phonons with MIM antennas made of heavily doped semiconductors. MIM antennas offer a simple way to control the energy of the gap-plasmon-phonon-polariton resonances. The strong confinement of the gap plasmon within the GaSb layer enables one to reach the ultrastrong coupling regime characterized here by a giant Rabi splitting of 30% of the TO-phonon energy.

[1] S. Collin, Rep. Prog. Phys. **77**, 126402 (2014).

[2] J. F. Federici, B. Schulkin, F. Huang, D. Gary, R. Barat, F. Oliveira, and D. Zimdars, Semicond. Sci. Technol. **20**, S266 (2005).

[3] G. Liang, X. Hu, X. Yu, Y. Shen, L. H. Li, A. Giles Davies, E. H. Linfield, H.-K. Liang, Y. Zhang, S.-F. Yu, and Q.-J. Wang, ACS Photonics **2**, 1559 (2015).

[4] E. Pickwell and V.-P. Wallace, J. Phys. D: Appl. Phys. **39**, R301 (2006).

[5] S. Koenig, D. Lopez-Diaz, J. Antes, F. Boes, R. Henneberger, A. Leuther, A. Tessmann, R. Schmogrow, D. Hillerkuss, R. Palmer, T. Zwick, C. Koos, W. Freude, O. Ambacher, J. Leuthold, and I. Kallfass, Nat. Photonics **7**, 977 (2013).

[6] H.-H. Chen, H.-H. Hsiao, H.-C. Chang, W.-L. Huang, and S.-C. Lee, Appl. Phys. Lett. **104**, 083114 (2014).

[7] M. G. Blaber, M. D. Arnold, and M. J. Ford, J. Phys: Condens. Matter **22**, 143201 (2010).

[8] A. J. Hoffman, L. Alekseyev, S. S. Howard, K. J. Franz, D. Wasserman, V. A. Podolskiy, E. E. Narimanov, D. L. Sivco, and C. Gmachl, Nat. Mater. **6**, 946 (2007).

[9] M. Fehrenbacher, S. Winnerl, H. Schneider, J. Doring, S. C. Kehr, L. M. Eng, Y. Huo, O. G. Schmidt, K. Yao, Y. Liu, and M. Helm, Nano Lett. **15**, 1057 (2015).

[10] A. N. Grigorenko, M. Polini, and K. S. Novoselov, Nat. Photonics **6**, 749 (2012).

[11] F. Barho, F. Gonzalez-Posada, M.-J. Milla-Rodrigo, M. Bomers, L. Cerutti, and T. Taliercio, Opt. Express **24**, 16176 (2016).

[12] J. Frigerio, A. Ballabio, G. Isella, E. Sakat, G. Pellegrini, P. Biagioni, M. Bollani, E. Napolitani, C. Manganelli, M. Virgilio, A. Grupp, M. P. Fischer, D. Brida, K. Gallacher, D. J. Paul, L. Baldassarre, P. Calvani, V. Giliberti, A. Nucara, and M. Ortolani, Phys. Rev. B **94**, 085202 (2016).

[13] S. Law, D. C. Adams, A. M. Taylor, and D. Wasserman, Opt. Express **20**, 12155 (2012).

[14] V. N'Tsame Guilengui, L. Cerutti, J. B. Rodriguez, E. Tournie, and T. Taliercio, Appl. Phys. Lett. **101**, 161113 (2012).

[15] G. M. Akselrod, C. Argyropoulos, T. B. Hoang, C. Ciraci, C. Fang, J. Huang, D. R. Smith, and M. H. Mikkelsen, Nat. Photonics **8**, 835 (2014).

[16] J. Hao, L. Zhou, and M. Qiu, Phys. Rev. B **83**, 165107 (2011).

[17] A. Moreau, C. Ciraci, J. J. Mock, R. T. Hill, Q. Wang, B. J. Wiley, A. Chilkoti, and D. R. Smith, Nature (London) **492**, 86 (2012).

[18] J. M. Manceau, S. Zanotto, I. Sagnes, G. Beaudoin, and R. Colombelli, Appl. Phys. Lett. **103**, 091110 (2013).

[19] A. Lefebvre, D. Costantini, I. Doyen, Q. Levesque, E. Lorent, D. Jacolin, J. J. Greffet, S. Boutami, and H. Benisty, Opt. Mater. Express **6**, 2389 (2016).

[20] M. G. Nielsen, A. Pors, O. Albrektsen, and S. I. Bozhevolnyi, Opt. Express **20**, 13311 (2012).

[21] J. Yang, C. Sauvan, A. Jouanin, S. Collin, J. L. Pelouard, and P. Lalanne, Opt. Express **20**, 16880 (2012).

[22] M. Miyata, A. Holsteen, Y. Nagasaki, M. L. Brongersma, and J. Takahara, Nano Lett. **15**, 5609 (2015).

[23] A. Shaltout, J. Liu, A. Kildishev, and V. Shalaev, Optica **2**, 860 (2015).

[24] A. Pors, O. Albrektsen, I. P. Radko, and S. I. Bozhevolnyi, Sci. Rep. **3**, 2155 (2013).

[25] C. Ciraci, R. T. Hill, J. J. Mock, Y. Urzhumov, A. I. Fernandez-Dominguez, S. A. Maier, J. B. Pendry, A. Chilkoti, and D. R. Smith, Science **337**, 1072 (2012).

[26] A. Moreau, C. Ciraci, and D. R. Smith, Phys. Rev. B **87**, 045401 (2013).

[27] J. Benedicto, R. Polles, C. Ciraci, E. Centeno, D. R. Smith, and A. Moreau, J. Opt. Soc. Am. A **32**, 1581 (2015).

[28] F. Omeis, R. Smaali, F. Gonzalez-Posada, L. Cerutti, T. Taliercio, and E. Centeno, Appl. Phys. Lett. **111**, 121108 (2017).

[29] S. Law, C. Roberts, T. Kilpatrick, L. Yu, T. Ribaudo, E. A. Shaner, V. Podolskiy, and D. Wasserman, Phys. Rev. Lett. **112**, 017401 (2014).

[30] C. Weisbuch, M. Nishioka, A. Ishikawa, and Y. Arakawa, Phys. Rev. Lett. **69**, 3314 (1992).

[31] P. G. Savvidis, J. J. Baumberg, R. M. Stevenson, M. S. Skolnick, D. M. Whittaker, and J. S. Roberts, Phys. Rev. Lett. **84**, 1547 (2000).

[32] D. Bajoni, P. Senellart, E. Wertz, I. Sagnes, A. Miard, A. Lemaître, and J. Bloch, Phys. Rev. Lett. **100**, 047401 (2008).

[33] A. F. Kockum, A. Miranowicz, S. De Liberato, S. Savasta, and F. Nori, Nat. Rev. Phys. **1**, 19 (2019).

[34] A. A. Anappara, S. De Liberato, A. Tredicucci, C. Ciuti, G. Biasiol, L. Sorba, and F. Beltram, Phys. Rev. B **79**, 201303(R) (2009).

[35] T. Niemczyk, F. Deppe, H. Huebl, E. P. Menzel, F. Hocke, M. J. Schwarz, J. J. Garcia-Ripoll, D. Zueco, T. Hümmer, E. Solano, A. Marx, and R. Gross, Nat. Phys. **6**, 772 (2010).

[36] V. M. Muravev, I. V. Andreev, I. V. Kukushkin, S. Schmult, and W. Dietsche, Phys. Rev. B **83**, 075309 (2011).

[37] T. Schwartz, J. A. Hutchison, C. Genet, and T. W. Ebbesen, Phys. Rev. Lett. **106**, 196405 (2011).

[38] J. George, T. Chervy, A. Shalabney, E. Devaux, H. Hiura, C. Genet, and T. W. Ebbesen, Phys. Rev. Lett. **117**, 153601 (2016).

[39] A. Thomas, L. Lethuillier-Karl, K. Nagarajan, R. M. A. Vergauwe, J. George, T. Chervy, A. Shalabney, E. Devaux, C. Genet, J. Moran, and T. W. Ebbesen, Science **363**, 615 (2019).

[40] D. J. Shelton, I. Brener, J. C. Ginn, M. B. Sinclair, D. W. Peters, K. R. Coffey, and G. D. Boreman, Nano Lett. **11**, 2104 (2011).

[41] C. Huck, J. Vogt, T. Neuman, T. Nagao, R. Hillenbrand, J. Aizpurua, A. Pucci, and F. Neubrech, Opt. Express **24**, 25528 (2016).

[42] W. Wan, X. Yang, and J. Gao, Opt. Express **24**, 12367 (2016).

[43] J. George, A. Shalabney, J. A. Hutchison, C. Genet, and T. W. Ebbesen, J. Phys. Chem. Lett. **6**, 1027 (2015).

[44] B. Askenazi, A. Vasanelli, A. Delteil, Y. Todorov, L. C. Andreani, G. Beaudoin, I. Sagnes, and C. Sirtori, New J. Phys. **16**, 043029 (2014).

[45] S. Huppert, A. Vasanelli, G. Pegolotti, Y. Todorov, and C. Sirtori, Phys. Rev. B **94**, 155418 (2016).

[46] D. W. Berreman, Phys. Rev. **130**, 2193 (1963).

[47] T. Weiss, G. Granet, N. A. Gippius, S. G. Tikhodeev, and H. Giessen, Opt. Express **17**, 8051 (2009).

[48] T. Taliercio, V. Ntsame Guilengui, L. Cerutti, E. Tournie, and J.-J. Greffet, Opt. Express **22**, 24294 (2014).

[49] S. Collin, F. Pardo, and J.-L. Pelouard, Opt. Express **15**, 4310 (2007).

[50] C. Lemaitre, E. Centeno, and A. Moreau, Sci. Rep. **7**, 2941 (2017).

[51] Y. Todorov, A. M. Andrews, R. Colombelli, S. De Liberato, C. Ciuti, P. Klang, G. Strasser, and C. Sirtori, Phys. Rev. Lett. **105**, 196402 (2010).